On the Efficiency of Collisional $O_2 + N_2$ Vibrational Energy Exchange

E. Garcia,*,† A. Kurnosov,‡ A. Laganà,¶ F. Pirani,¶ M. Bartolomei,§ and M. Cacciatore‖

Departamento de Quimica Fisica, Universidad del Pais Vasco (UPV/EHU), 01006 Vitoria, Spain, Troitsk Institute of Innovation and Fusion Research, 142092 Troitsk, Moscow, Russia, Dipartimento di Chimica, Biologia e Biotecnologie, Università di Perugia, 06100 Perugia, Italy, Instituto de Física Fundamental, CSIC, Serrano 117, 28006 Madrid, Spain, and Nanotec - Institute for Nanotechnology CNR c/o University campus, Chemistry Department, Via Orabona 4, 70123 Bari, Italy

E-mail: e.garcia@ehu.es

*To whom correspondence should be addressed
†Departamento de Quimica Fisica, Universidad del Pais Vasco (UPV/EHU), 01006 Vitoria, Spain
‡Troitsk Institute of Innovation and Fusion Research, 142092 Troitsk, Moscow, Russia
¶Dipartimento di Chimica, Biologia e Biotecnologie, Università di Perugia, 06100 Perugia, Italy
§Instituto de Física Fundamental, CSIC, Serrano 117, 28006 Madrid, Spain
‖Nanotec - Institute for Nanotechnology CNR c/o University campus, Chemistry Department, Via Orabona 4, 70123 Bari, Italy

Abstract

By following the scheme of the Grid Empowered Molecular Simulator (GEMS) a new $O_2 + N_2$ intermolecular potential, built on ab initio calculations and experimental (scattering and second virial coefficient) data, has been coupled with an appropriate intramolecular one. On the resulting potential energy surface detailed rate coefficients for collision induced vibrational energy exchanges have been computed using a semi-classical method. The crossed comparison of the computed rate coefficients with the outcomes of previous semiclassical calculations and kinetic experiments has provided a ground for characterizing the main features of the vibrational energy transfer processes of the title system as well as a critical reading of the trajectory outcomes and kinetic data. On the implemented procedures massive trajectory runs for the proper interval of initial conditions have singled out structures of the vibrational distributions useful to formulate scaling relationships for complex molecular simulations.

Keywords

Oxygen nitrogen collisions, bond-bond interaction, potential energy surface, V-V energy transfer, V-T energy transfer, semiclassical methods, quasiclassical trajectory methods

1 Introduction

The characterization of the kinetics of elementary chemical processes (both in terms of evaluating detailed rate coefficients (RC) and in terms of quantifying the energy interplay among different degrees of freedom of the involved system) is a key challenge for molecular research. In particular, among the aspects that need to be better characterized in this respect, is the suitability of the adopted formulation of the Potential Energy Surface (PES) to deal properly with Vibration-to-Vibration (V-V) and Vibration-to-Translation (V-T) energy transfer in gas phase collisions.

Our interest for V-V and V-T energy exchange in non reactive collisions between oxygen and nitrogen molecules having different vibrational energy content has been stimulated by the recently re-emphasized importance of such kind of processes for the development of innovative aerospace technologies.[1–4] Our investigation focuses, in particular, on the accurate radial and angular modulation of the interaction (both at long and short range) of the collision partners and on the contribution given by the different state specific RCs to the measured overall efficiency of vibrational quenching and to the implementation of complex simulations.

The workflow model adopted in our investigation is the distributed synergistic one of the Grid Empowered Molecular Simulator (GEMS)[5,6] (mainly in charge to AL and EG). The first module of GEMS (INTERACTION) is devoted to the production and/or collection of the necessary high level ab initio information on the electronic structure of the system while the second module of GEMS (FITTING) is devoted to the (combined theory and experiment) optimization of the parameters of a semiempirical PES (mainly in charge to MB and FP). The third module of GEMS (DYNAMICS) is devoted to the production of massive detailed dynamical information to feed the fourh module (OBSERVABLES) that carries out their statistical handling aimed at building more averaged measurable quantities (such as cross sections and rate coefficients). In this way the efficiency of the investigated processes can be quantified and related models and representations can be built[7–9] (mainly in charge to MC, AK and EG).

GEMS has been already specialized in the past for the systematic study of the efficiency of V-V and V-T processes in the case of the N_2 + N_2 system.[10,11] In this paper we discuss the application of such workflow to the case of the O_2–N_2 system. In particular, the INTERACTION module is used for collecting and/or producing high level ab initio electronic structure data for an accurate characterization of the key regions of the O_2–N_2 interaction. The determination of the parameters of the adopted functional form, allowing the assemblage of a robust global PES (named MF) more solidly grounded on accurate ab initio calculations, is performed in the FITTING module and compared with the one (GB1)

already used in the literature for SemiClassical (SC) calculations.[12] The running on both MF and GB1 PESs of systematic distributed SC computations for the evaluation of the V-V and V-T state-to-state probabilities is carried out in the DYNAMICS module using the same quantum-classical technique. Next, the efficiency of the two surfaces in promoting V-V and V-T energy transfer is systematically compared in the OBSERVABLES module by calculating the detailed RCs and developing a rationale for understanding the discrepancies between theoretical and measured vibrational quenching. A further iteration of the computational procedures of the DYNAMICS and OBSERVABLES modules using Quasi-Classical Trajectory (QCT) techniques is performed in order to extend the investigation to higher vibrational states and higher temperatures (so as to work out appropriate parameters for enabling scaling procedures in massive aerothermodynamics simulations).

In this way three basic objectives are targeted: the characterization of the effect of improving the functional representation of the intermolecular interaction on the calculated value of the RCs; the better understanding of some limits of the use of QCT techniques in V-V and V-T energy transfer studies (with respect to semiclassical calculations and the experiment); the exploitation of the use of distributed computing workflows for massive studies of V-V and V-T energy transfers by extending the calculations to different vibrational states and temperature values.

Accordingly, the paper is articulated as follows: In section 2 the new potential energy surface is formulated and its parameters are optimized, in section 3 the outcomes of the semiclassical calculations performed on the GB1 and MF PESs are compared and used to the end of rationalizing the experiment, in section 4 the limits and benefits of extending the calculation domain using quasiclassical methods are discussed, in section 5 some conclusions are drawn.

2 The O_2–N_2 potential energy surface

As typical of the calculations on the efficiency of energy transfer processes in molecule molecule collisions, the overall interaction V is partitioned in an *intra* and an *inter* component

$$V = V_{intra} + V_{inter}. \tag{1}$$

The GB1 V_{inter} is formulated as a combination of short (SR) and long range (LR) terms.[12] The SR components are expressed as exponentials in the first and second power of the R_{ij} internuclear distance of the ij atomic pairs involved while the LR component is expressed as a sum of a permanent quadrupole-permanent quadrupole electrostatic interaction truncated to the first term plus an attractive dispersion component.

The MF V_{inter} is formulated, instead, as a combination of two "effective" (see below) improved bond-bond components (made of a van der Waals V_{vdW} and an electrostatic term V_{elect}). This makes it more flexible (and accurate) and allows an optimization of its parameters aimed at reproducing to high level ab initio values of the O_2–N_2 interaction (computed for the molecular geometries associated with the evolution of the different arrangements of the system during the collision process) and available scattering properties estimated using detailed dynamical methods. To this end, the modules of GEMS were iteratively used by performing alternate accurate ab initio calculations and calibrations of the PES parameters.

V_{intra} is for both GB1 and MF formulated as a sum of Morse potentials[13] in which the N_2 one has a dissociation energy of 9.90517 eV (228.4181 kcal/mol), an equilibrium distance of 1.09768 Å and an exponential parameter of 2.68867 $Å^{-1}$ while the O_2 one has a dissociation energy of 5.21319 eV (120.2187 kcal/mol), an equilibrium distance of 1.20752 Å and an exponential parameter of 2.65374 $Å^{-1}$.

2.1 The bond-bond representation of the MF PES

The MF V_{inter} of the two O_2 and N_2 interacting structured bodies is formulated as a combination

$$V_{inter} = V_{vdW} + V_{elect} \tag{2}$$

of the two "effective" interaction components V_{vdW} and V_{elect} representing the van der Waals (size repulsion plus dispersion attraction) and the electrostatic interaction terms, respectively.[14] The V_{vdW} term is formulated as a bond-bond pair-wise interaction (that is more appropriate than the traditional atom-atom one) because it leverages on the additivity of the bond polarizability in contributing to the overall (molecular) one. This is a fundamental feature of the vdW interactions and accounts indirectly for three body like effects.[15] The V_{elect} term is instead formulated as an electrostatic interaction associated with an anisotropic distribution of the molecular charge over the two interacting bodies (say molecule a and b) that asymptotically tends to the permanent quadrupole – permanent quadrupole interaction.

Both V_{vdW} and V_{elect} depend on the intermolecular distance R between the centers of mass of molecule a and b (let us take a for O_2 and b for N_2), on the Jacobi angles Θ_a and Θ_b formed by $\mathbf{R}$ with the internuclear vectors $\mathbf{r}_a$ and $\mathbf{r}_b$, respectively, and the angle Φ the dihedral angle formed by the planes $(\mathbf{R}, \mathbf{r}_a)$ and $(\mathbf{R}, \mathbf{r}_b)$. In this paper we focus our attention on the (Θ_a,Θ_b,Φ) = (90°,90°,0°), (90°,90°,90°), (90°,0°,0°), (0°,90°,0°) and (0°,0°,0°) configurations, which are referred to as H (D_{2h}), X (D_{2d}), T_a (C_{2v}), T_b (C_{2v}) and I ($D_{\infty h}$) with related group symmetry being given in brackets.

The formulation adopted for the van der Waals term V_{vdW} is of the Improved Lennard-Jones (ILJ) type:[16]

$$V_{vdW}(R,\gamma) = \varepsilon(\gamma)\left[\frac{6}{n(x)-6}\left(\frac{1}{x}\right)^{n(x)} - \frac{n(x)}{n(x)-6}\left(\frac{1}{x}\right)^{6}\right] \tag{3}$$

often used in its reduced form

$$f(x) = \frac{V_{vdW}(R,\gamma)}{\varepsilon(\gamma)} \tag{4}$$

where x is the reduced distance of the two bodies defined as

$$x = \frac{R}{R_m(\gamma)} \tag{5}$$

and γ denotes collectively the triplet of angles $(\Theta_a, \Theta_b, \Phi)$, while ε and R_m are respectively the fixed γ well depth of the interaction potential and the equilibrium value of R.

The key feature of the ILJ functional form is the adoption of the additional (variable) exponential parameter n providing more flexibility than the usual Lennard-Jones(12,6) (LJ) one thanks to its dependence on both R and γ as:[16,17]

$$n(x) = \beta + 4.0\ x^2 \tag{6}$$

in which β is a parameter depending on the nature and the hardness of the interacting particles leading to a more realistic representation of both repulsion (first term in square brackets of Eq. 3) and attraction (second term in square brackets of Eq. 3). For the present system β has been set equal to 9 (a value typical of van der Waals interactions in neutral-neutral systems).[16]

Additional flexibility is given to V_{vdW} by expanding ε and R_m in terms of the bipolar spherical harmonics $\mathrm{A}^{L_1L_2L}(\gamma)$. In this way $f(x)$ (the already mentioned reduced form of the bond-bond potential[17]) is taken to be the same for all the relative orientations, as already discussed in Refs. 18–21. This way of introducing the angular dependence of the potential parameters provides a convergence of V_{vdW} much faster than that of its direct expansion in terms of radial coefficients.[14,22–24] For the purpose of the present work it was found sufficient to truncate the expansion to the fifth order, as follows:

$$\varepsilon(\gamma) = \varepsilon^{000} + \varepsilon^{202}A^{202}(\gamma) + \varepsilon^{022}A^{022}(\gamma) + \varepsilon^{220}A^{220}(\gamma) + \varepsilon^{222}A^{222}(\gamma) \tag{7}$$

$$R_m(\gamma) = R_m^{000} + R_m^{202} A^{202}(\gamma) + R_m^{022} A^{022}(\gamma) + R_m^{220} A^{220}(\gamma) + R_m^{222} A^{222}(\gamma). \quad (8)$$

A method to estimate the value of the ε and R_m expansion parameters from diatomic (or molecular bond) polarizability values is illustrated in Appendix A of Ref. 14. Accordingly, once ε and R_m are determined for the five selected geometries of the bond-bond pair, the coefficients $\varepsilon^{L_1 L_2 L}$ and $R_m^{L_1 L_2 L}$ can be worked out by inversion of Eqs. 7 and 8.[14,22,25] In this way a suitable tentative full dimensional PES is generated. Further optimization of the ε and R_m values obtained by fitting experimental data and accurate ab initio electronic structure calculations will be discussed in the next subsection.

In the study reported here, as already done for the N_2 + N_2 system,[14] the V_{elect} term of Eq. 2 has been formulated by only retaining the main quadrupole-quadrupole contribution and, for this purpose, use has been made of the expression

$$V_{elect}(R, \gamma) = \frac{Q_a Q_b}{R^5} A^{224}(\gamma) \quad (9)$$

where Q_a and Q_b are, as usual, the diatomic permanent quadrupole moments. Q terms have been evaluated using ab initio calculations and have been accurately fitted to a fifth order polynomial for both monomers in order to introduce their dependence on r_a and r_b.

2.2 Details of the optimization procedure of the MF PES parameters

As already mentioned, the initial values of the parameters of the monomers estimated at their equilibrium internuclear distance from the corresponding polarizability tensor components to the end of building the bond-bond MF PES were optimized (within a limited range) to better reproduce the ab initio interaction energies,[26] the measured integral cross sections[27] and the second virial coefficients.[28,29]

The key experimental data used in our investigation aimed to optimize the parameters of the MF PES is the total integral cross section (Q) (see Ref. 27) of the scattering of

rotationally hot and near effusive O_2 beams by N_2 molecules measured as a function of the beam velocity v. $Q(v)$ data (shown in the upper panel of Fig. 1) exhibiting an oscillatory pattern (the glory structure) are known to provide accurate information on the intermolecular interaction involved.[16] At low and intermediate translational energy, in fact, the collision mainly probes the absolute scale of the isotropic component of the interaction while at high translational energy the collision mainly probes the strength of the anisotropic one (see Ref. 30 and references therein).

In the thermal energy range these measurements have been found to be reproduced with high accuracy by JWBK calculations.[31] The JWKB calculations quoted here have been performed using both a spherical average of the interaction[30] and the (fast rotating O_2) pseudoatom – (rotationally cold N_2) diatom limiting Infinite Order Sudden Approximation (IOSA) scheme.[18] The values of the total cross section $Q(v)$ (computed both on the ab initio PES and on the MF one) are plotted in the upper panel of Fig. 1 after convolution from the center of mass to the laboratory frame.

The optimization resulting from the best fit of the second virial coefficient $B(T)$ has been obtained by computing its value at different temperatures T using the semiclassical procedure for two linear molecules.[32] The formula incorporate the first quantum correction due to the relative translational and rotational motions, including Coriolis coupling. The computed values are compared in the lower panel of Fig. 1 with the experimental data of Refs. 28 and 29.

It is worth pointing out here, again, that, given the physical ground of the optimization procedure, both the number of parameters allowed to vary and their range of variation are limited. As an example, the long range dispersion attraction coefficient values, defined as εR_m^6 in the ILJ model, were allowed to vary within an interval of 10% of their initial value (see also Appendix A of Ref. 14).

The detailed comparison between present predictions and the available experimental data (reported in the upper and lower panel of Fig. 1 for integral cross sections and second virial

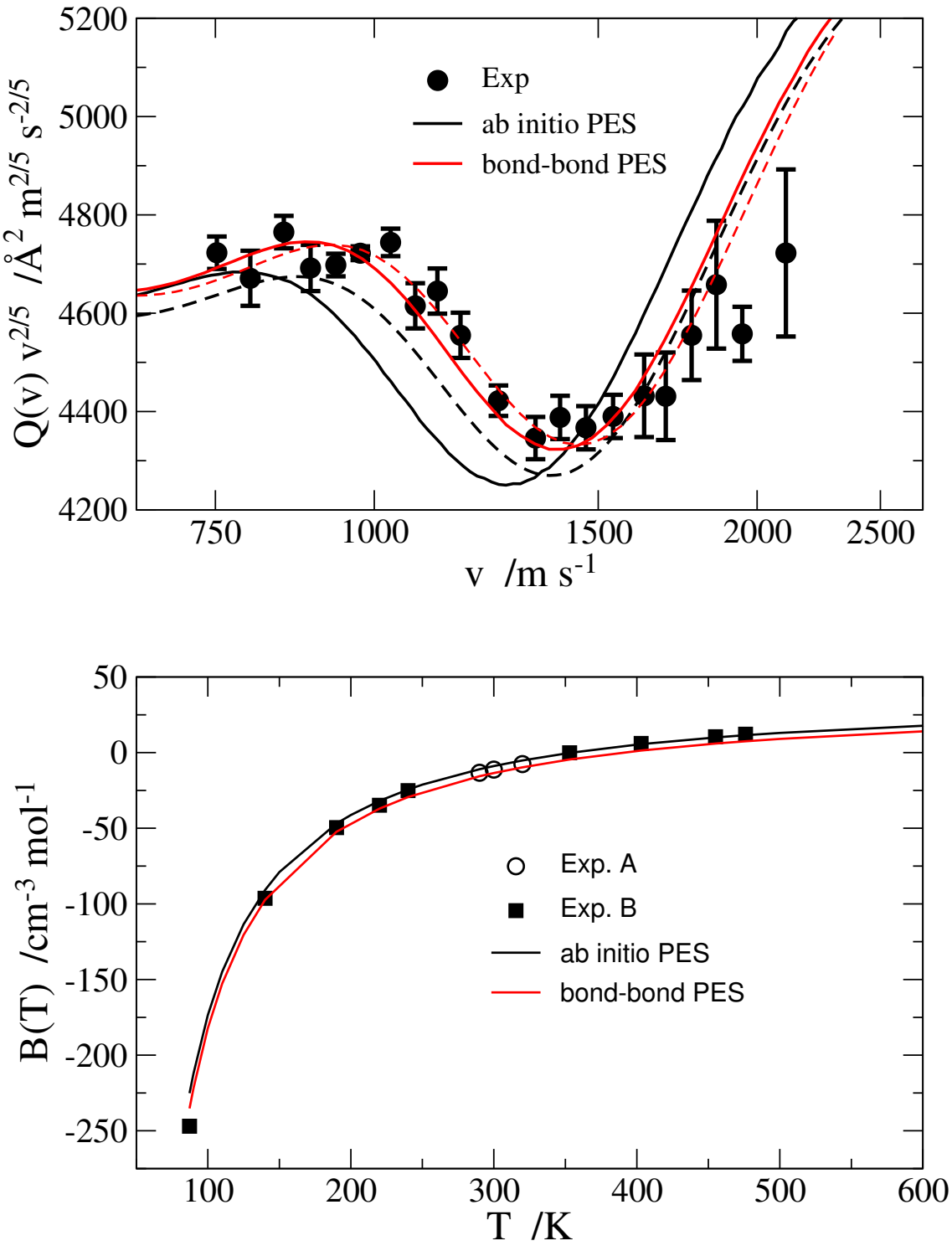

Figure 1: Upper panel: Total integral cross sections $Q(v)$ times $v^{2/5}$, for the scattering of a rotationally hot O_2 effusive beam by N_2 target molecules, plotted as a function of the beam velocity, v. Full and dashed lines represent calculations using the spherical and the pseudoatom-diatom interaction, respectively. Lower panel: Second virial coefficient $B(T)$ plotted as a function of temperature.

coefficients, respectively) includes also the estimates obtained on the ab initio PES.[26] As to the integral cross section, the calculations well reproduce the experimental average absolute value of the glory pattern as well as its position and amplitude in the low and intermediate collision velocity range. The effect of the interaction anisotropy exalted at high velocity and producing the already mentioned partial glory quenching, is taken into account within the pseudoatom-diatom limit. As to the second virial coefficient, the results of the computations provide a good agreement (within the experimental uncertainties) with the measured data. Finally, it is also interesting to note that the pseudoatom-diatom limiting behavior of the present intermolecular PES is similar to that of the Ar–N_2 interaction[19] offering further ground for theoretical considerations on the fact that O_2 exhibits an isotropic polarizability consistent with that of Ar.

As already mentioned, the optimization of the ε and R_m parameters was performed using ab initio calculations of the intermolecular interaction energies as well as integral cross section and second virial coefficient data. Ab initio calculations for the five selected geometries of the title system were performed at SAPT(DFT) (symmetry-adapted perturbation theory) level utilizing a density functional description of the monomers and a large basis set.[26] The optimized values for the case of monomers at their equilibrium internuclear distance are given in Table 1.

Table 1: Parameters of the bond-bond MF PES

L_1	L_2	L	$\varepsilon^{L_1L_2L}$	$R_m^{L_1L_2L}$
0	0	0	12.2760[a]	3.8014[b]
2	0	2	-1.3918	0.1529
0	2	2	-0.9892	0.1289
2	2	0	0.0995	0.0047
2	2	2	-0.0832	-0.0039

[a] in meV; [b] in Å

As previously anticipated, the optimized bond-bond MF values and the accurate ab initio values of Ref. 26 are here used as reference results. The adopted optimization procedure led,

in fact, to a highly reliable MF PES valid in the whole space of the explored configurations. The cuts[14,26] of the resulting PES taken by considering the monomers at their equilibrium internuclear distance while approaching in their X (D_{2d}), H (D_{2h}), T_a (C_{2v}), T_b (C_{2v}) and I ($D_{\infty H}$) arrangements, are plotted in Fig. 2. It is worth pointing out here that two T-shaped arrangements are considered separately: T_a, where the O_2 intramolecular vector $\mathbf{r}_a$ is perpendicular to $\mathbf{R}$, and T_b, where N_2 diatom vector $\mathbf{r}_b$ is oriented perpendicularly to $\mathbf{R}$. As apparent from the figure the bond-bond MF PES satisfactorily reproduces the ab initio features of the interactions including the depth and position of the minimum of the potential wells for all the arrangements as well as for their spherical average. However, it has to be noticed that the wells of the more repulsive T_a, T_b and I configurations are shallower and the well depth of the corresponding spherical average is about 10% deeper and located at shorter (about 0.2 Å) distances.

Figure 2 shows also the potential profiles of the GB1 PES. In general, the potential wells of the bond-bond MF PES are deeper and have a minimum located at shorter distances than those of GB1. A discussion on how this affects the values of the RCs computed on the different PESs will be given later. However, a recent paper demonstrates the increasing role of the attraction portion of V_{inter} in the control of RC values when decreasing the temperature of the bulk.[33]

3 The dynamical study

The first goal of our dynamical study was targeted to the evaluation of the RC computed on the two PESs (MF and GB1) using the semiclassical coupled state method.

3.1 The semiclassical coupled state method

The key feature of the adopted SC coupled state method (see Refs. 34 and 35 for a more extended discussion) is that molecular vibrations are treated quantum-mechanically by inte-

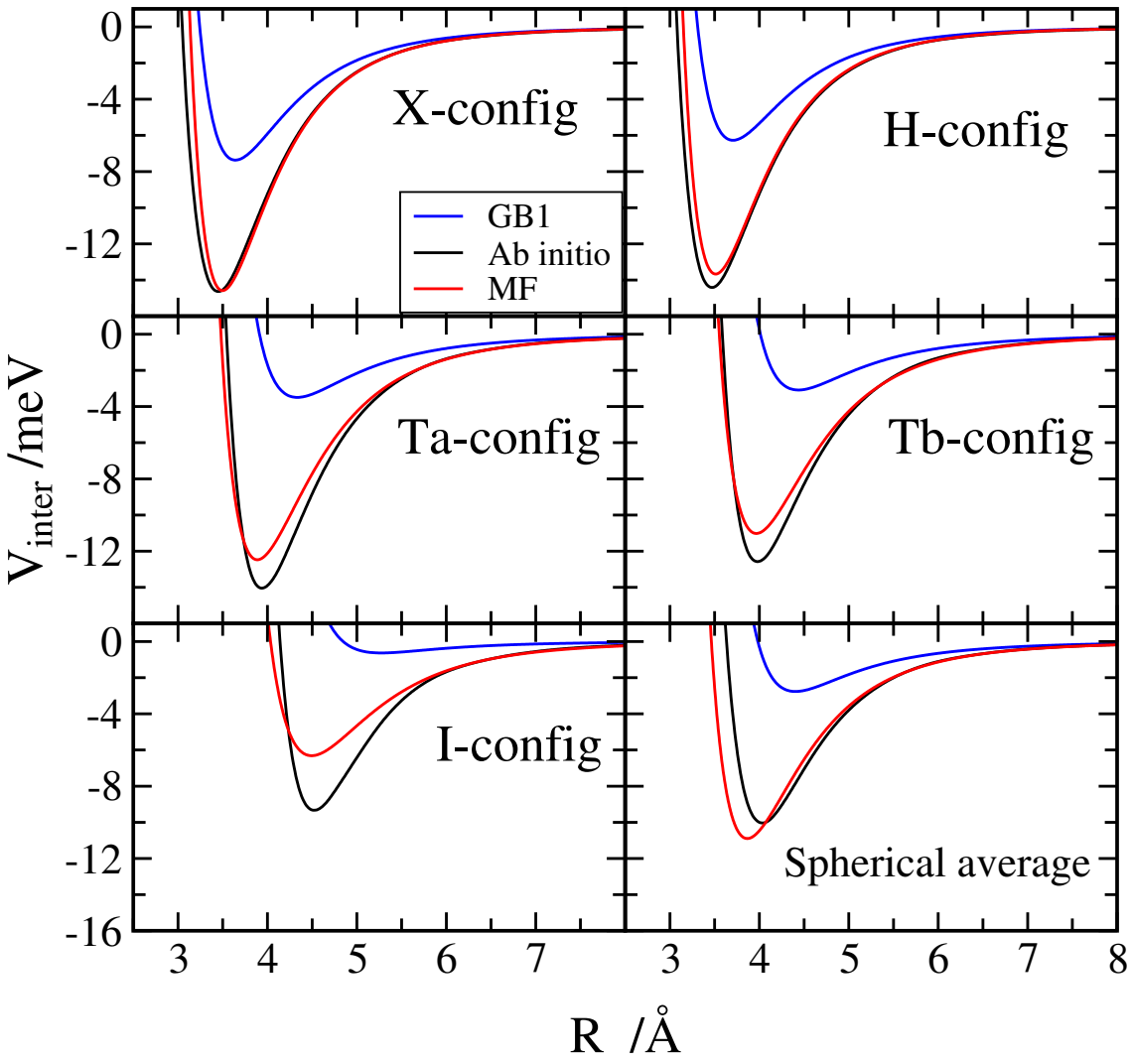

Figure 2: Potential energy profiles of GB1, ab initio and MF PESs plotted as a function of R for the X, H, T_a, T_b and I arrangements of the O_2–N_2 dimer with the monomers at their equilibrium internuclear distance. In the bottom rhs panel the spherical average of the PESs is also shown.

grating the related time-dependent Schrödinger equations for the N_2 and the O_2 molecules. On the contrary, translational and rotational degrees of freedom are treated classically by integrating the related classical Hamilton equations. The two subsystems, and the corresponding equations of motion, are dynamically coupled through the definition and calculation of a time-dependent "effective" Hamiltonian, of the Ehrenfest type, defined as the expectation value of the intermolecular interaction potential over $\Psi(r_a, r_b, t)$:

$$H_{\text{eff}} =< \Psi(r_a, r_b, t) \mid V_{inter}(R(t)) \mid \Psi(r_a, r_b, t) > \tag{10}$$

where $V_{inter}(R(t))$ is the intermolecular interaction potential evaluated at each time step of the classical "mean" trajectory $R(t)$.

The time evolution of the total wave function is obtained by expanding $|\Psi(r_a, r_b, t)>$ over the manifold of the product, rotationally-distorted, Morse wave functions of the two isolated molecules $\Phi_{v'_a}(r_a, t)$ and $\Phi_{v'_b}(r_b, t)$ as follows:

$$\Psi(r_a, r_b, t) = \sum_{v'_a, v'_b} \Phi_{v'_a}(r_a, t)\ \Phi_{v'_b}(r_b, t)\ \exp\left[-i\frac{E_{v'_a} + E_{v'_b}}{\hbar}\ t\right]\ A_{v_a v_b \rightarrow v'_a v'_b}(t) \tag{11}$$

in which $A_{v_a v_b \rightarrow v'_a v'_b}(t)$ is the amplitude of the vibrational transition from v_a and v_b to v'_a and v'_b, $E_{v'_i}(t)$ is the eigenvalue of the v'_i Morse wavefunction $\Phi_{v'_i}(r_i, t)$ corrected by the Coriolis coupling elements $H_{v''_a v'_b}$

$$\Phi_{v'_i}(r_i, t) = \Phi^0_{v'_i}(r_i) + \sum_{v''_i \neq v'_i} \Phi^0_{v''_i}(r_i)\frac{H_{v''_i v'_i}}{E^0_{v'_i} - E^0_{v''_i}} \tag{12}$$

The second term in Eq. 12 represents the first-order centrifugal stretching contribution coupling rotations and vibrations of diatom with $\Phi^0_{v'_i}$ and $E^0_{v'_i}$ being the eigenfunction and the eigenvalue, respectively, of the same Morse oscillator. In the same equation

$$H_{v''_i v'_i} = -j_i^2(t) v_i^{''-1} (\overline{r}_i)^{-3} < \Phi^0_{v''_i} | r_i - \overline{r}_i | \Phi^0_{v'_i} > \tag{13}$$

with j_i being the rotational momentum of molecule i whose equilibrium distance is $\overline{r}_i$.

Thus, the Hamilton equations for the roto-translational motions are integrated self-consistently together with the Schrödinger equations of the vibrational amplitudes. We solve $(2N + 18)$ coupled classical (18) and quantum $(2N)$ equations with N being the total number of vibrational levels in the total wave function expansion. The number of vibrational levels, above and below the initial vibrational state of N_2 and O_2, included in the wave function expansion depends on the initial vibrational state of both molecules and on the impact kinetic energy. The higher are the impact energy and the level of vibrational excitations of N_2 and O_2, the greater the number of vibrational states to include (and, therefore, the larger is the number of coupled wave equations to be solved). At the same time the calculations need to be repeated for a set of N_t trajectories sufficient to sample adequately the diatomic rotational angular momentum range of initial values (for both a and b, from 0 to $j_{a\max}$ and $j_{b\max}$ respectively) as well as the diatom – diatom orbiting angular momentum range of initial values (from 0 to $l_{\max}$).

Accordingly, the semiclassical cross section for the vibrational transition $v_a v_b \to v'_a v'_b$ (or $(v_a, v_b|v'_a, v'_b)$) is given by the following expression:

$$\sigma_{v_a v_b \to v'_a v'_b}(U) = \frac{\pi \hbar^6}{8\mu I_a I_b (k_{\mathrm{B}} T_0)^3} \int_0^{l_{\max}} \mathrm{d}l \int_0^{j_{a\max}} \mathrm{d}j_a \int_0^{j_{b\max}} \mathrm{d}j_b \, \frac{[l j_a j_b]}{N_{v_a v_b}} \sum |A_{v_a v_b \to v'_a v'_b}|^2 \quad (14)$$

in which $[l j_a j_b] = (2j_a + 1)(2j_b + 1)(2l + 1)$, U is the classical part of the kinetic energy ($U = E_{kin} + E^a_{rot} + E^b_{rot}$) with E_{kin} being the impact kinetic energy, E^i_{rot} and I_i being the rotational energy and the related moment of inertia of molecule i, μ and l being the reduced mass and the orbital angular momentum, respectively, of the colliding system and k_{B} the Boltzmann constant. In the same expression T_0 is an arbitrary reference temperature introduced in order to provide the proper dimensionality to the cross section expression.

The state-to-state rate coefficients are then obtained by averaging over an initial Boltz-

mann distribution of kinetic and rotational energies:

$$k_{v_a v_b \to v'_a v'_b}(T) = \sqrt{\frac{8k_{\mathrm{B}}T}{\pi\mu}} \left(\frac{T_0}{T}\right)^3 \int_{\varepsilon_{\min}}^{\infty} \sigma_{v_a v_b \to v'_a v'_b}(U)\ \exp\left[-\frac{\overline{U}}{k_{\mathrm{B}}T}\right]\ \mathrm{d}\left(\frac{\overline{U}}{k_{\mathrm{B}}T}\right) \qquad (15)$$

where $\overline{U}$ is the symmetrized effective energy ($\overline{U} = U + \frac{1}{2}\Delta E + \Delta E^2/16U$), with E being the total energy and $\Delta E = E_{v'_a} + E_{v'_b} - E_{v_a} - E_{v_b}$ being the energetic balance.

3.2 Semiclassical calculations

A first comparison of the SC RC values obtained on the MF PES can be carried out with those obtained on GB1[12] at $T = 300$ K (see Table 2). The total number N_t of integrated trajectories, sufficient to assure numerical convergence of the calculated vibrational amplitudes and cross-sections for each considered value of U in the interval $0.025 - 7.440$ eV, was found to be 1000. From the calculated cross sections the detailed RC ($k_{v_a v_b \to v'_a v'_b}(T)$ when possible indicated for sake of brevity as $(v_a, v_b|v'_a, v'_b)$) obtained by averaging over the relevant cross sections. In the Table, SC RCs for vibrational energy transfer from $O_2(v_a = 13, 19, 25)$ + $N_2(v_b = 0)$ to $O_2(v'_a)$ + $N_2(v'_b)$ are shown. It is worth to point out here that the MF and the GB1 SC results for V-V and V-T transitions differ appreciably (with those calculated on MF being on average one order of magnitude smaller than the ones calculated on GB1).

Table 2: SC GB1 (upper row) and MF (lower row) rate coefficients (in cm^3 s^{-1}) at $T = 300$ K

v_a, v_b	$v'_a = v_a - 2$ $v'_b = v_b + 1$	$v'_a = v_a - 1$ $v'_b = v_b$	$v'_a = v_a - 1$ $v'_b = v_b + 1$	$v'_a = v_a - 2$ $v'_b = v_b$
13,0	5.9(-16)	3.5(-16)	4.0(-20)	8.0(-19)
	4.5(-16)	9.6(-17)	3.7(-21)	8.1(-20)
19,0	5.1(-15)	3.3(-15)	1.4(-20)	1.5(-17)
	2.5(-15)	9.9(-16)	5.0(-22)	1.5(-18)
25,0	4.2(-16)	1.6(-14)	4.7(-21)	2.3(-16)
	1.0(-16)	7.9(-15)	3.0(-22)	2.7(-17)

Such comparison when extended to higher temperatures (see Table 3 for the SC RC

values computed at $T = 1000$ K) confirms again that SC RCs computed on GB1 are larger than those computed on MF (almost, on the average, one order of magnitude) and show that V-T transitions (second and last columns) are at least one order of magnitude more efficients than V-V ones.

Table 3: SC GB1 (upper row) and MF (lower row) rate coefficients (in cm^3 s^{-1}) at $T = 1000$ K

v_a, v_b	$v'_a = v_a - 2$ $v'_b = v_b + 1$	$v'_a = v_a - 1$ $v'_b = v_b$	$v'_a = v_a - 1$ $v'_b = v_b + 1$	$v'_a = v_a - 2$ $v'_b = v_b$
13,0	4.7(-15)	3.3(-13)	7.4(-16)	8.5(-15)
	2.2(-15)	6.1(-14)	3.0(-17)	5.6(-16)
19,0	2.2(-14)	1.3(-12)	3.7(-16)	5.0(-14)
	7.3(-15)	3.0(-13)	1.5(-17)	6.7(-15)
25,0	1.2(-14)	3.5(-12)	3.7(-16)	3.9(-13)
	3.1(-15)	1.1(-12)	1.6(-17)	6.0(-14)

3.3 A comparison with experimental data

The computed values of the $O_2(v_a) + N_2(v_b = 0) \rightarrow O_2(v'_a = v_a - 2) + N_2(v'_b = 1)$ SC RC can be suitably plotted as a function on v_a so as to illustrate the efficiency of vibrational state specific near resonant V-V processes. This is, indeed, what is shown in Fig. 3 where related SC RCs computed both on GB1 and MF are plotted together with the corresponding experimental results of Ref. 36. It is noteworthy to point out here that not only the SC RCs calculated on MF are smaller than the ones calculated on GB1 but they appear significantly smaller than the quoted experimental results. The points here to understand are therefore (a) why MF results are systematically smaller than the GB1 ones, and (b) why theoretical results are systematically smaller than experimental data.

As to item (a) it is instructive to inspect the convergence process of the calculation of the cross section of Eq. 14. It shows that the main contributions to it come on GB1 at distances larger than on MF. This is in line with the fact that, as shown in Fig. 2, the repulsive wall of the GB1 PES is located at larger distances and even a simple hard sphere model (assuming

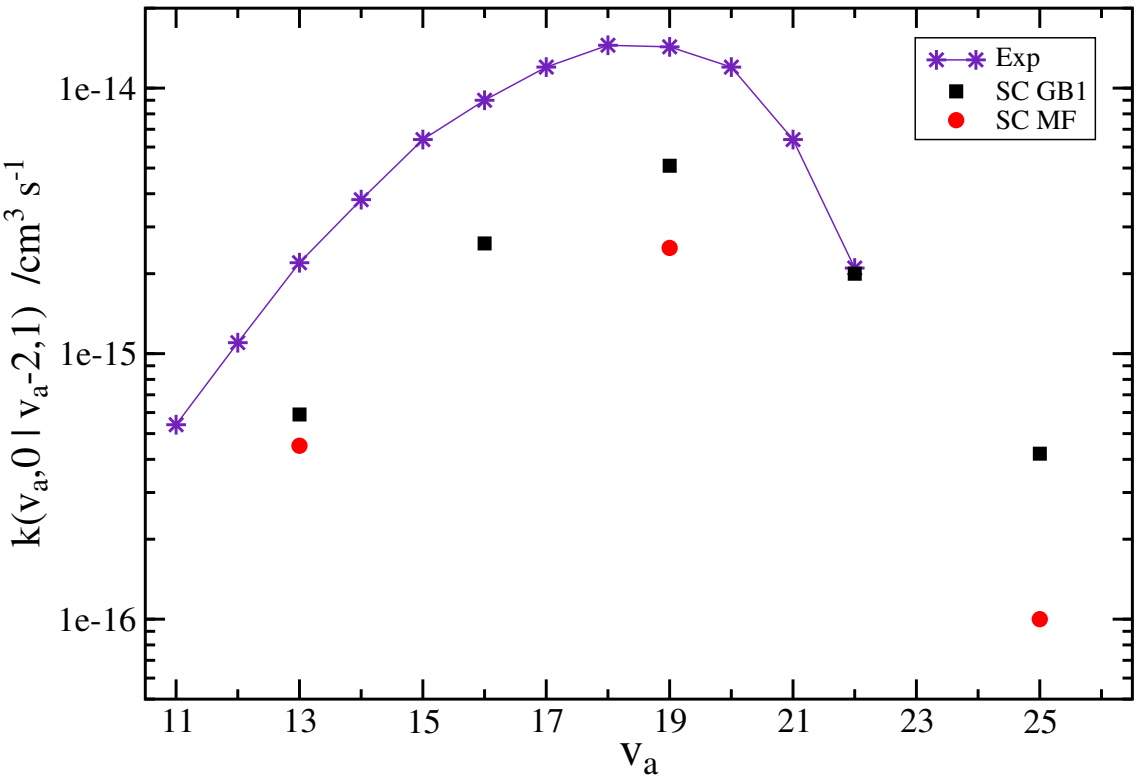

Figure 3: Comparison between the $O_2(v_a) + N_2(v_b = 0) \rightarrow O_2(v'_a = v_a - 2) + N_2(v'_b = 1)$ SC rate coefficients at $T = 300$ K calculated on and MF with corresponding experimental results of Ref. 36.

that the quasi resonant V-V transfer occurs at the collision turning point) would give a difference between the GB1 and the MF cross section of about 30%. Such rationalization is supported by the plot of the SC RC as a function of T in the interval of temperature ranging up to 1000 K (see Fig. 4). The Figure clearly shows that the GB1 V-V transfer is systematically larger than the MF ones (though it lowers as T decreases as already found for $N_2 + N_2$ in Ref. 10)

As to item (b) a first point to make is that the $v_a = 19$ process, $O_2(v_a = 19) + N_2(v_b = 0) \rightarrow O_2(v'_a = 17) + N_2(v'_b = 1)$, is near resonant (while the other V-V processes and the V-T ones are not). For this process it is maintained in ref. 12 that, at the temperature of the considered experiment, V-T transitions are expected to be negligible (though about two times more efficient than those of pure oxygen). Despite that, V-T related RCs have been used to the end of working out a value of the V-V ones.[36] Critical to this is the fact that, in the above quoted papers, mention is made not only to a significant increase of the V-T contribution to vibrational quenching for the above transition, as temperature increases (especially at higher v values) but also to the fact that such contribution is more than appreciable already at 300 K. Despite the fact that the author of ref. 12 attributes the discrepancy between theory and experiment to an inadequacy of the used PES, the lack of reactive channels in both GB1 and MF makes the best of the experimental data available. After all, the fact that a more reliable PES (such as the MF one that is solidly based on ab initio calculations and a multiproperty analysis) leads to a lower V-V RC makes it reasonable the conclusion that the real value of the related rate coefficient should be smaller.

A case for further comparison of theoretical and experimental data is given by the SC calculations performed at low vibrational states, namely involving molecules in the $v = 0$ and 1 initial states. Table 4 shows the temperature evolution of the SC RCs for the lowest single quantum V-V and V-T transitions calculated using Eq. 15 and adopting the collisional approach on MF. Also these results further confirm that SC calculations give RC estimates smaller than those of the experiment.[37] In particular, the RC of the V-V $O_2(v_a = 1) +$

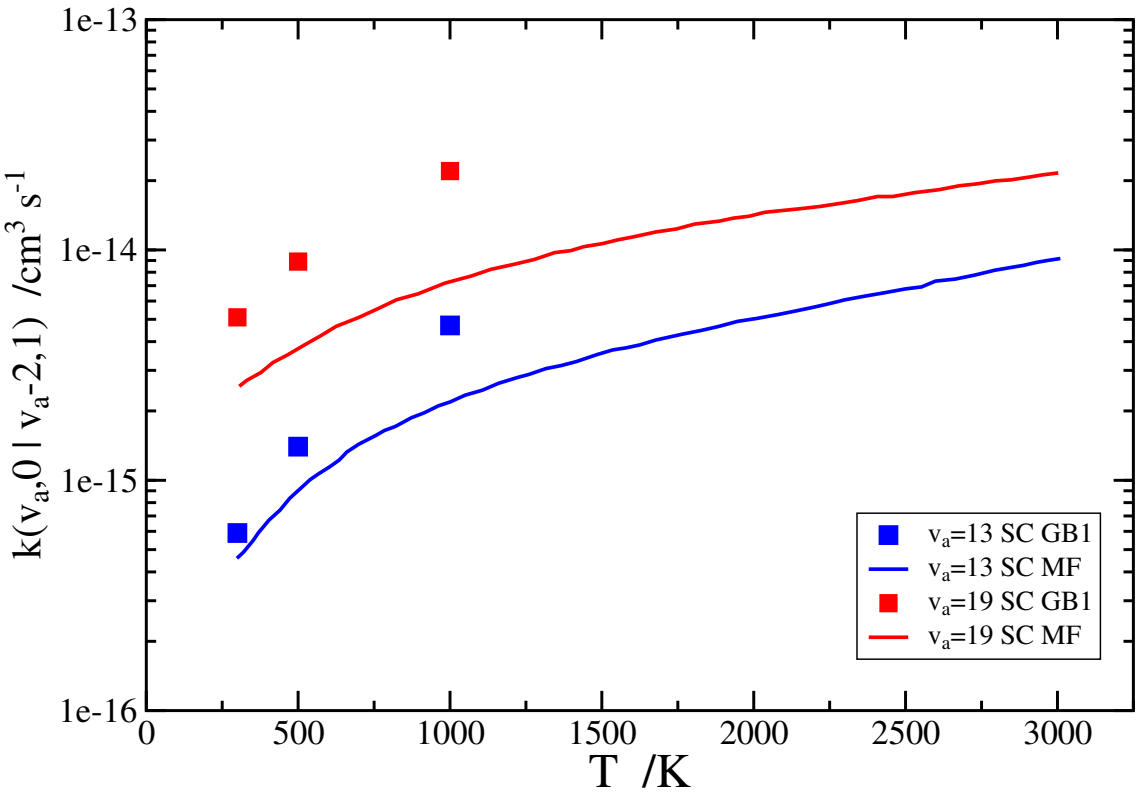

Figure 4: SC rate coefficients calculated on GB1 and MF at $v_a = 13$ and 19 plotted as a function of temperature.

$N_2(v_b = 0) \rightarrow O_2(v'_a = 0) + N_2(v'_b = 1)$ exchange process at $T = 800$ K is estimated from the experiment to be 7.27(-16) cm^3 s^{-1} while its calculated value is 3.91(-23) cm^3 s^{-1}. Yet, as found also for the larger v transitions already considered, the SC RC for the $O_2(v_a = 0) + N_2(v_b = 1) \rightarrow O_2(v'_a = 0) + N_2(v'_b = 0)$ transition that contributes to the V-T process, is five orders of magnitude larger. This allows us to conclude that the underestimation of the experimental data is mainly due to the fact that the phenomenological equation proposed in Ref. 37 is dominated by non V-V processes.

Table 4: SC MF rate coefficients (in cm^3 s^{-1}) for some $(v_a, v_b|v'_a, v'_b)$ transitions involving lowest vibrational states

T/K	$(0,1\|1,0)$	$(1,0\|0,1)$	$(0,1\|0,0)$
300	4.61(-25)	1.13(-26)	5.19(-21)
500	9.26(-25)	9.99(-26)	3.03(-20)
700	8.44(-24)	1.72(-24)	2.72(-19)
800	3.91(-23)	9.74(-24)	7.17(-19)
1000	6.94(-22)	2.28(-22)	3.76(-18)
2000	1.83(-18)	1.05(-18)	5.10(-16)
3000	7.65(-17)	5.28(-17)	6.46(-15)
5000	4.96(-15)	3.97(-15)	1.02(-13)
7000	4.70(-14)	4.00(-14)	5.07(-13)

4 Additional dynamical studies

To the end of extending the domain of the investigation of the energy transfer mechanisms to higher vibrational states and temperatures, we resorted into using massive QCT calculations which are easily implementable on the Grid. QCT calculations, in fact, have been already shown to be able to fully exploit the enhanced grid capacity of GEMS[38–42] and to be able to cut the average computing time of a factor equal to half the number of nodes used.

4.1 Quasiclassical trajectory calculations

As to the QCT results, a preliminary comment is in order to motivate why we made these additional calculations. The key reason is, as mentioned above, the wish of going beyond the memory and compute time limitations affecting SC approaches. This is particularly true when pushing the calculations to higher vibrational states closer to dissociation (it is important to emphasize here the fact that this has also dictated the adaptation of the bond-bond functional formulation of the MF PES aimed at accurately describe the stretching of the diatomic bonds up to the dissociation limit), extend the temperature to higher values and increase the number and size of the compute tasks distributed on the Grid for massive calculations to the end of producing complete tables of state to state RCs for use by sophisticated molecular simulations.

In this perspective we carried out on the mentioned PESs (MF and GB1) massive QCT calculations using the VENUS program.[43] This was after all the original motivation for designing GEMS from the very beginning and for its recent specialization in simulating the measured signal of Crossed Molecular Beam (CMB) experiments using classical mechanics means.[44] CMB experiments are performed using narrow distributions of reactant collision energy around its nominal value and a selected set of rovibrational states. Accordingly the theoretical and computational apparatus is targeted to estimate the product number density associated with a given set of initial conditions. This quantity can be evaluated directly if one knows the experimental machine setting and we have developed in Perugia single stream procedures standardizing the offer of related services on the web.[38–42,44] The procedure relies on (partially) the interconnecting of theoretical predictions with the measured signal thanks to the support of automated workflows allowing the coordinated usage of several packages. It also relies on the community supported access to a vast quantity of distributed compute resources. All this has become feasible thanks to the support of the European Grid Infrastructure (EGI)[45] and well fits with its Service Oriented Architecture (SOA)[46] philosophy. In particular, the use of VENUS in the DYNAMICS module of GEMS for the

purpose of the present paper is particularly appropriate because the code is ideally suited for distributing massive trajectory calculations.

The calculated quantities are the inelastic vibrational state-to-state rate coefficients $k_{v_a v_b \to v'_a v'_b}(T)$:

$$k_{v_a v_b \to v'_a v'_b}(T) = \sqrt{\frac{8 k_{\mathrm{B}} T}{\pi \mu}}\, \pi b_{\max}^2\, \frac{N_{v_a v_b, v'_a v'_a}}{N_{v_a v_b}} \tag{16}$$

where k_{B} is the Boltzmann constant, μ is the reduced mass of the system, $\pi b_{\max}^2 N_{v_a v_b, v'_a v'_b}/N_{v_a v_b}$ is the QCT cross section with $b_{\max}$ being the maximum value taken by the impact parameter and $N_{v_a v_b, v'_a v'_b}$ being the subset of the total number of trajectories $N_{v_a v_b}$ computed starting from states v_a and v_b and ending into states v'_a and v'_b.

At low vibrational numbers QCT calculations with O_2 and N_2 molecules vibrationally excited do not show appreciable vibrational energy transfer probability. In fact, out of 50 millions trajectories run for both $O_2(v = 1) + N_2(v = 0)$ and $O_2(v = 0) + N_2(v = 1)$ at 300 K none of them were found to be effective in transferring vibrational energy. This did set in these cases a bottom value (of $6.6(-18)$ cm^3 s^{-1}) below which no QCT RCs could be computed. This limit of QCT techniques does not allow to estimate smaller energy transfer RCs.

4.2 Quasiclassical versus semiclassical calculations

For higher vibrationally excited colliding molecules it is, however, still meaningful to perform systematic QCT calculations. This is indeed what we did for O_2 molecule having $v_a = 13$, 19 and 25 colliding with the N_2 molecule in its ground vibrational state, $v_b = 0$, on the GB1 and MF PESs. Initial collisional energies and rotational states (including the different degeneration for even and odd states of the N_2 molecule due to the nuclear spin of the nitrogen atom) were instead selected according to the Boltzmann distribution at the considered temperature T. The temperature values considered were $T = 300$ and 1000 K. At $T = 300$ K 100 millions of trajectories were run for each v_a initial value while at

$T = 1000$ K 50 millions of trajectories were run at $v_a = 13$ and 20 millions at $v_a = 19$ and 25. No vibrational transitions as a result of the collision were found for the N_2 molecule, confirming the inadequacy of the QCT method for evaluating vibrational energy exchange at low vibrational number and temperatures.

RC values computed at $T = 300$ K show that the QCT treatments lead to no vibrational energy transfer for $v_a = 13$ on both GB1 and MF PESs. For $v_a = 19$, instead, only on GB1 a single quantum transition is detected and its value is almost two order of magnitude smaller than the related SC one ($4.9(-17)$ *versus* $3.3(-15)$ cm^3 s^{-1}, see Table 2). This further confirms the previously commented higher V-V exchange efficiency when the repulsive wall of V_{inter} is displaced to larger distances. As the initial vibrational excitation of O_2 increases up to $v_a = 25$ the agreement between QCT and SC calculations improves on GB1 ($9.2(-15)$ *versus* $1.6(-14)$ cm^3 s^{-1} for the $(25, 0|24, 0)$ transition and $3.0(-17)$ *versus* $3.3(-16)$ cm^3 s^{-1} for the $(25, 0|23, 0)$ transition). Moreover, at $v_a = 25$, a single quantum vibrational deexcitation is found on MF even though the QCT RC is significantly smaller than the related SC value ($2.9(-16)$ *versus* $7.9(-15)$ cm^3 s^{-1}).

$T = 1000$ K QCT RCs computed on both the GB1 and MF PES are shown in Table 5. The same values are also plotted in Figure 5 together with the related SC ones computed on both GB1 and MF. As apparent from the Figure, QCT results reasonably well reproduce the behavior of the SC ones. In fact, single quantum vibrational deexcitation (upper panel of the Figure) SC and QCT RCs calculated on GB1 show a good agreement at $v_a = 13$ and this agreement worsens as v_a increases while on MF the QCT RC well reproduces the SC one at $v_a = 19$ underestimating (overestimating) the SC value at $v_a = 13$ ($v_a = 25$). It is worth to note that the dependence of the single quantum vibrational deexcitation RC on the initial vibrational excitation of O_2 calculated using the QCT method is slightly larger than that found on the SC results for both GB1 and MF PESs, being the former rates larger, as already mentioned. The conclusions found for the single quantum vibrational deexcitation of O_2 can be extended to the double quantum vibrational deexcitation (lower panel of the

Figure) even though in this case the discrepancies between the QCT and SC RCs are larger due to the smaller values of the QCT RCs.

Table 5: QCT GB1 (upper row) and MF (lower row) rate coefficients (in cm^3 s^{-1}) at $T = 1000$ K

v_a, v_b	$v'_a = v_a - 1$ $v'_b = v_b$	$v'_a = v_a - 2$ $v'_b = v_b$
13,0	3.3(-13)	8.5(-15)
	6.1(-14)	5.6(-16)
19,0	2.2(-14)	5.0(-14)
	7.3(-15)	3.0(-13)
25,0	1.2(-14)	3.5(-12)
	3.1(-15)	1.1(-12)

4.3 Quasiclassical results scaling

The enhanced features of GEMS enabling massive runs of distributed QCT calculations offers the advantage of obtaining in short times the full batch of results needed for implementing accurate complex molecular simulations. Accordingly, once aware of the limits of acceptability of QCT calculations, we investigated the possibility of figuring out scaling rules for an automatic usage of the results collected from massive grid calculations by merging information obtained from different computational tasks.

For illustrative purposes, we discuss here in some detail the $T = 1000$ K case of both GB1 and MF results. As already mentioned at $T = 1000$ K QCT results become reliable enough to allow an analysis (see Fig. 6) of the O_2 molecule multiquantum vibrational transitions (with no vibrational excitation of the N_2 molecule). As apparent form the Figure the rate coefficients for the vibrational excitation of O_2 are non negligible. In fact, for $v_a = 19$ and 25 (and even for $v_a = 13$) the single vibrational excitation rate is as high as 50% of the related deexcitation value. Indeed, for the double quantum vibrational excitation when initially O_2 is in $v = 19$ and 25 RCs are approximately 30% larger than the corresponding double deexcitation value.

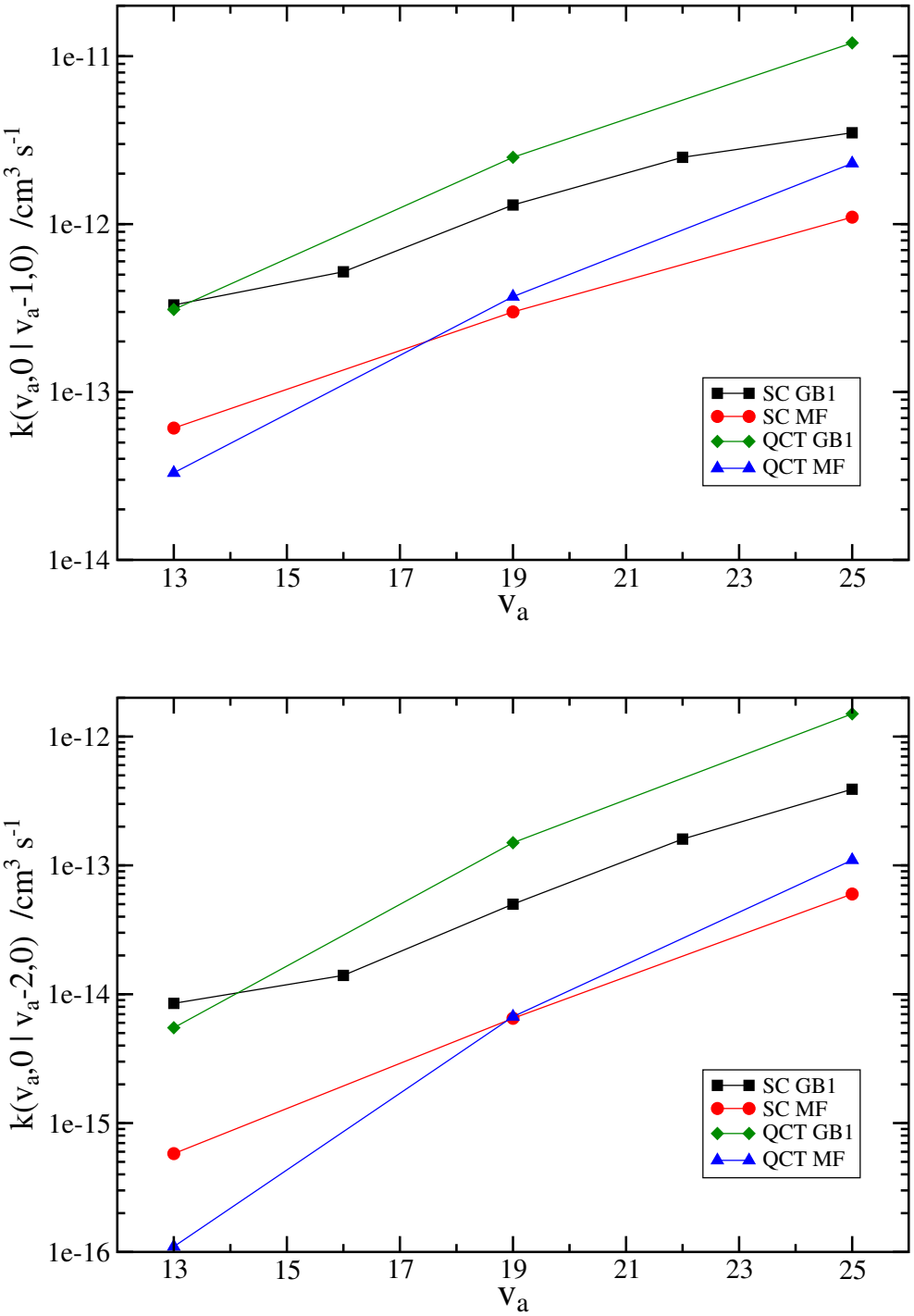

Figure 5: SC and QCT rate coefficients at $T = 1000$ K calculated on GB1 and MF for single (upper panel) and double (lower panel) quantum vibrational deexcitation of the process $O_2(v_a) + N_2(v_b = 0) \rightarrow O_2(v'_a) + N_2(v'_b = 0)$

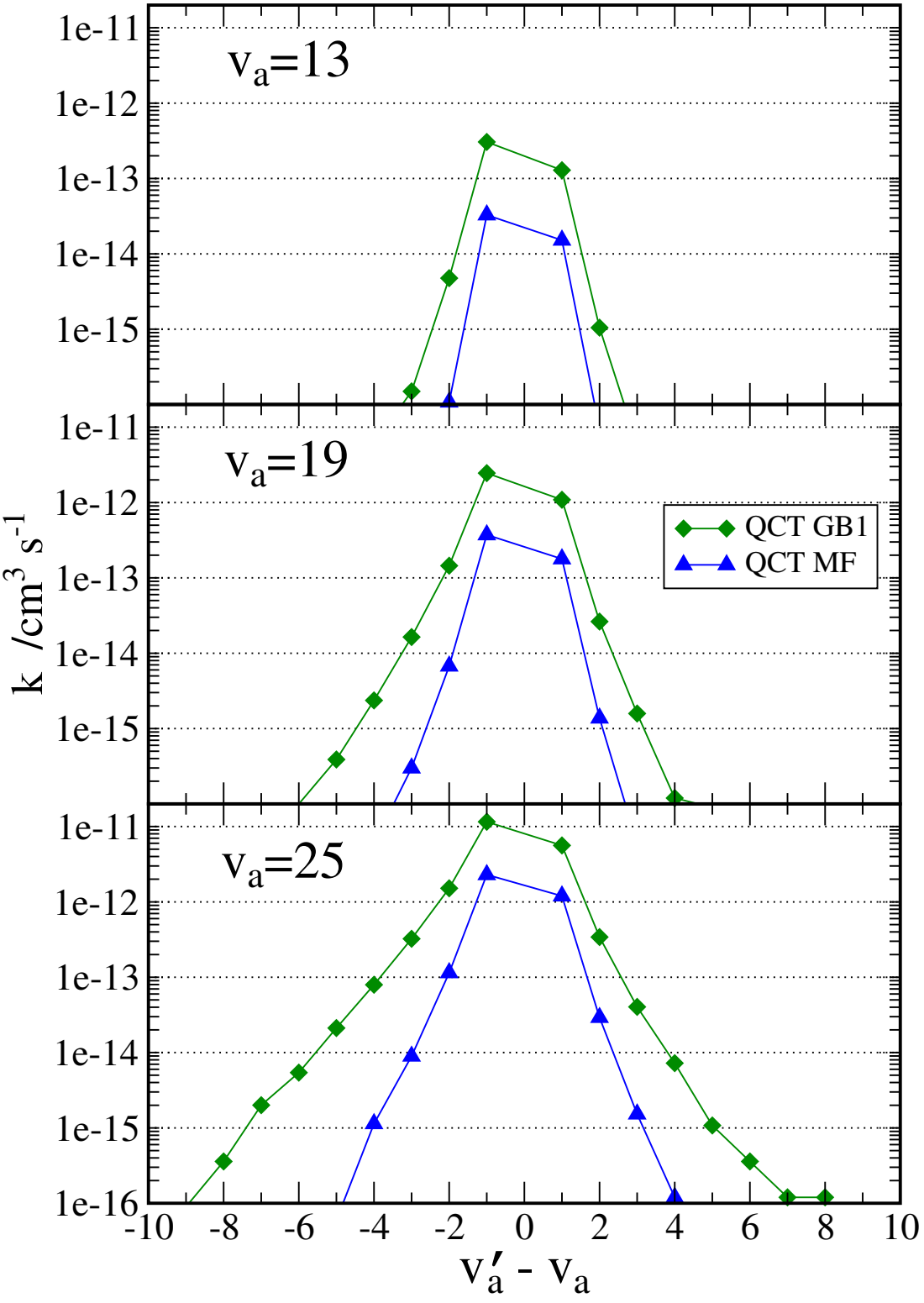

Figure 6: QCT rate coefficients at $T = 1000$ K calculated on GB1 and MF for multiquantum vibrational excitation and deexcitation of the process $O_2(v_a) + N_2(v_b = 0) \rightarrow O_2(v'_a) + N_2(v'_b = 0)$

This singles out how important is the lesson one can take home from the detailed inspection of Fig. 6: using the GEMS grid workflow it is easy to pile up in a database the most accurate possible QCT RC values and exploit the related scaling rules to build more accurate (like the SC or even full quantum when possible) set of estimates. RC plots show, in fact, a nice smooth asymmetric gaussian-like shape that can be easily parametrized as a function of the the initial and final vibrational state as well as of temperature and then applied to quantum and SC data. These scaling rules are at present being automated also for similar diatom-diatom systems.

5 Conclusions

The use of a synergistic approach to the computational study of molecular processes presented in this paper has shown to be challenging and fruitful for several reasons. The first reason is that the cooperative model of the GEMS scheme allowed us to complement each other our research experience and expertise in an a workflow articulated fashion. The construction of the PES sprouted out from the combined usage of ab initio calculations, detailed scattering data and iterative optimization of the parameters of a suitable functional formulation of the potential. The second reason is that the comparison of the dynamical outcomes, computed on two PESs using a well consolidated semiclassical and quasiclassical techniques, and their rationalization as well in terms of both a long range attractive tail and a repulsive wall of the used PES, provided us with a support that enabled to infer that measurements are highly affected by V-T contributions. The third reason is that the comparative analysis of the SC and QCT RC values computed on the optimized MF PES, while setting precise limits to the usability of classical mechanics treatments, opens a huge field of applicability to the realistic modeling of complex gas phase systems thanks developing scaling rules through which feed estendend detailed data bases of RCs. Furthermore the specific study of the O_2 + N_2 collisional vibrational energy exchange processes reported here will serve as a basis for

extending the use of GEMS to the investigation of systems containing vibrationally excited oxygen and nitrogen molecules for their relevance in phenomena occuring in aerospace, in could plasmas and in the upper atmosphere, where for example they can compete with the collisions $O+O_2$[47] in the spacecraft reentry to Earth or with the $e^- + O_2 + N_2 \rightarrow O + N_2$ three body electron attachment, an important process of electron removal in the earth atmosphere.[48]

Acknowledgement

The authors acknowledge financial support from the Phys4entry FP7/2007-2013 project (Contract 242311), ARPA Umbria, INSTM, the EGI-Inspire project (Contract 261323), MIUR PRIN 2008 (2008KJX4SN 003) and 2010/2011 (2010ERFKXL_002), the ESA-ESTEC contract 21790/08/NL/HE and the Spanish CTQ2012-37404 and FIS2013-48275-C2-1-P projects. Computations have been supported by the use of Grid resources and services provided by the European Grid Infrastructure (EGI) and the Italian Grid Infrastructure (IGI) through the COMPCHEM Virtual Organization. Thanks are also due to the COST CMST European Cooperative Project CHEMGRID (Action D37) EGI Inspire.

References

(1) Lino da Silva, M.; Guerra, V.; Loureiro J. A Review Of Non-Equilibrium Dissociation Rates And Models For Atmospheric Entry Studies. *Plasma Sources Sci. Technol.* **2009**, *18*, 34023-34034.

(2) Coitout, H.; Cernogora, G. Experimental Study Of The Temporal Evolution Of $N_2(C^3\Pi_u)$ And $N_2(B^3\Pi_g)$ In A Nitrogen Pulsed Discharge. *J. Phys. Chem. D: Appl. Phys.* **2006**, *39*, 1821-1829.

(3) Kurnosov, A.; Napartovich, A.; Shnyrev, S.; Cacciatore, M. Vibrational Energy Ex-

changes In Nitrogen: Application Of The New Rate Constants For Kinetic Modeling. *J. Phys. Chem. A* **2007**, *111*, 7057-7065.

(4) Molecular Physics and Hypersonic Flows M.Capitelli Ed., Kluver Academic Publishers, Norwell, M.A., 1996

(5) Costantini, A.; Gutierrez, E.; López-Cacheiro, J.; Rodríguez, A; Gervasi, O.; Laganà, A. On The Extension Of The Grid Empowered Molecular Science Simulator: MD And Visualization Tools. *Int. J. Web Grid Serv.* **2010**, *6*, 141-159.

(6) Costantini, A.; Gervasi, O.; Manuali, C.; Faginas-Lago, N.; Rampino, S.; Laganà, A. COMPCHEM: Progress Towards GEMS A Grid Empowered Molecular Simulator And Beyond. *J. Grid Comput.* **2010**, *8*, 571-586.

(7) Storchi, L.; Tarantelli, F.; Laganà, A. Computing Molecular Energy Surfaces On The Grid. *Lect. Notes Comput. Sc.* **2006**, *3980*, 675-683.

(8) Manuali, C.; Rampino, S.; Laganà, A. GRIF: A Grid Framework For A Web Service Approach To Reactive Scattering. *Comp. Phys. Comm.* **2010**, *181*, 1179-1185.

(9) Costantini, A.; Laganà, A.; Pirani, F.; Maris, A.; Caminati, W. Ab Initio And Empirical Atom-Bond Formulation Of The Interaction Of Dimethyleter-Ar System. *Lect. Notes Comput. Sc.* **2005**, *3482*, 1046-1053.

(10) Kurnosov, A.; Cacciatore, M.; Laganà, A.; Pirani, F.; Bartolomei, M.; Garcia, E. The Effect Of The Intermolecular Potential Formulation On The State-Selected Energy Exhange Rate Coefficients In The N_2-N_2 Collisions. *J. Comput. Chem.* **2014**, *35*, 722-736.

(11) Garcia, E.; Martínez, T.; Laganà, A. Quasi Resonant Vibrational Energy Transfer In N_2 + N_2 Collisions: Effect Of The Long Range Interaction. *Chem. Phys. Lett.* **2015**, *620*, 103-108.

(12) Billing, G. D. VV and VT rates in N_2-O_2 collisions. *Chem. Phys.* **1994**, *179*, 463-467.

(13) Huber, K. P.; Herzberg, G. *Molecular Spectra and Molecular Structure, Vol. IV: Constants of Diatomic Molecules*; Van Nostrand Reinhold: New York, 1979.

(14) Cappelletti, D.; Pirani, F.; Bussery-Honvault, B.; Gomez, L.; Bartolomei, M. A Bond-Bond Description Of The Intermolecular Interaction Energy: The Case Of Weakly Bound N_2-H_2 And N_2-N_2 Complexes. *Phys. Chem. Chem. Phys.* **2008**, *10*, 4281-4293.

(15) Pirani, F.; Cappelletti, D.; Liuti, G. Range Strength And Anisotropy Of The Intermolecular Forces In Atom-Molecule Systems: An Atom-Bond Pairwise Additivity Approach. *Chem. Phys. Lett.* **2001**, *350*, 286-296.

(16) Pirani, F.; Brizi, S.; Roncaratti, L. F.; Casavecchia, P.; Cappelletti, D.; Vecchiocattivi, F. Beyond The Lennard-Jones Model: A Simple And Accurate Potential Energy Function Probed By High Resolution Scattering Data Useful For Molecular Dynamics Simulations. *Phys. Chem. Chem. Phys.* **2008**, *10*, 5489-5503.

(17) Pirani, F.; Albertí, M.; Castro, A.; Moix-Teixidor, M.; Cappelletti, D. An Atom -Bond Pairwise Additive Representation For Intermolecular Potential Energy Surfaces. *Chem. Phys. Lett.* **2004**, *394*, 37-44.

(18) Pack, R. T. Anisotropic Potentials And The Damping Of Rainbow And Diffraction Oscillations In Differential Cross Sections. *Chem. Phys. Lett.* **1978**, *55*, 197-201.

(19) Candori, R.; Pirani, F.; Vecchiocattivi, F. The N_2-Ar Potential Energy Surface. *Chem. Phys. Lett.* **1983**, *102*, 412-415.

(20) Beneventi, L.; Casavecchia, P.; Volpi, G. G. HighâĂŘResolution Total Differential Cross Sections For Scattering Of Helium By O_2, N_2, And NO. *J. Chem. Phys.* **1986**, *85*, 7011-7029.

(21) Beneventi, L.; Casavecchia, P.; Pirani, F.; Vecchiocattivi, F.; Volpi, G. G.; Brocks, G.; van der Avoird, A.; Heijmen, B.; Reuss, J. The Ne-O_2 Potential Energy Surface From High Resolution Diffraction And Glory Scattering Experiments And From The Zeeman Spectrum. *J. Chem. Phys.* **1991**, *95*, 195-204.

(22) Bartolomei, M.; Cappelletti, D.; de Petris, G.; Moix-Teixidor, M.; Pirani, F.; Rosi, M.; Vecchiocattivi, F. The Intermolecular Potential In NO-N_2 And (NO-N_2)+Systems: Implications For The Neutralization Of Ionic Molecular Aggregates. *Phys. Chem. Chem. Phys.* **2008**, *10*, 5993-6001.

(23) Karimi-Jafari, M. H.; Ashouri, M.; Yeganeh-Jabri, A. Coping With The Anisotropy In The Analytical Representation Of An Ab Initio Potential Energy Surface For The Cl_2 Dimer. *Phys. Chem. Chem. Phys.* **2009**, *11*, 5561-5568.

(24) Bartolomei, M.; Pirani, F.; Laganà, A.; Lombardi, A. A full dimensional grid empowered simulations of the CO_2-CO_2 processes. *J. Comput. Chem.* **2012**, *33*, 1806-1819.

(25) Gomez, L.; Bussery-Honvault, B.; Cauchy, T.; Bartolomei, M.; Cappelletti, D.; Pirani, F. Global Fits Of New Intermolecular Ground State Potential Energy Surface For N_2-H_2 And N_2-N_2 Van Der Waals Dimers. *Chem. Phys. Lett.* **2007**, *445*, 99-107.

(26) Bartolomei, M.; Carmona-Novillo, E.; Hernández, M. I.; Campos-Martínez, J.; Moszynski, R. Global Ab Initio Potential Energy Surface For The $O_2(^3\Sigma^-)$ + $N_2(^1\Sigma^+)$ Interaction. Applications To The Collisional, Spectroscopic, And Thermodynamic Properties Of The Complex. *J. Phys. Chem. A* **2014**, *118*, 6584-6594.

(27) Brunetti, B.; Liuti, G.; Luzzatti, E.; Pirani, F.; Vecchiocattivi, F. Study Of The Interactions Of Atomic And Molecular Oxygen With O_2 And N_2 By Scattering Data. *J. Chem. Phys.* **1981**, *74*, 6734-6741.

(28) Martin, M.; Trengove, R.; Harris, K.; Dunlop, P. Excess Second Virial Coefficients For Some Binary Gas Mixtures. *Aust. J. Chem.* **1982**, *35*, 1525-1529.

(29) Fostiropoulos, K.; Natour, G.; Sommer, J.; Schramm, B. Die Zweiten Virialkoeffizienten Der Systeme N_2âĂŞO_2 Und N_2âĂŞNO Von 87 K Bzw. 124 K Bis 475 K. *Ber. Bunsenges. Phys. Chem.* **1988**, *92*, 925-930.

(30) Aquilanti, V.; Bartolomei, M.; Carmona-Novillo, E.; Pirani, F. The Asymmetric Dimer N_2-O_2: Characterization Of The Potential Energy Surface And Quantum Mechanical Calculation Of Rotovibrational Levels. *J. Chem. Phys.* **2003**, *118*, 2214-2222.

(31) Aquilanti, V.; Ascenzi, D.; Cappelletti, D.; de Castro, M.; Pirani, F. Scattering Of Aligned Molecules : The Potential Energy Surfaces For Kr-O_2 And Xe-O_2 Systems. *J. Chem. Phys.* **1998**, *109*, 3898-3910.

(32) Pack, R. T. 1st Quantum Corrections To 2nd Virial-Coefficients For Anisotropic Interactions - Simple, Corrected Formula. *J. Chem. Phys.* **1983**, *78*, 7217-7222.

(33) Martínez, R. Z.; Bermejo, D. Experimental Determination Of The Rate Of VâĂŞV Collisional Relaxation In $^{14}N_2$ In Its Ground ($X^1\Sigma_g^+$) Electronic State Between 77 And 300 K. *Phys. Chem. Chem. Phys.* **2015**, *17*, 12661-12672.

(34) Billing, G. D. Semiclassical Theory For Diatom-Diatom Collisions. *Chem. Phys. Lett.* **1983**, *97*, 188-192.

(35) Cacciatore, M.; Kurnosov, A.; Napartovich, A. Vibrational Energy Transfer In N_2-N_2 Collisions: A New-Semiclassical Study. *J. Chem. Phys.* **2005**, *123*, 174315-174325.

(36) Park H.; Slanger T. G. O_2(X,v=8-22) 300 K Quenching Rate Coefficients For O_2 And N_2, And O_2(X) Vibrational Distribution From 248 nm O_3 Photodissociation. *J. Chem. Phys.* **1994**, *100*, 287-300.

(37) Gilmore, F. R.; Bauer, E.; McGowan, J. W. A Review Of Atomic And Molecular Excitation Mechanisms In Nonequilibrium Gases Up To 20000 K. *J. Quant. Spectrosc. Radiat. Transfer* **1969**, *9*, 157-183.

(38) Costantini, A.; Laganà, A.; Pirani, F. Parallel Calculation Of Propane Bulk Properties. *Lect. Notes Comput. Sc.* **2006**, *3980*, 738-743.

(39) Costantini, A.; Faginas-Lago, N.; Laganà, A.; Huarte-Larrañaga F. A Grid Implementation Of Direct Semiclassical Calculations Of Rate CoeïňČcients. *Lect. Notes Comput. Sc.* **2009**, *5593*, 93-103.

(40) Costantini, A.; Laganà, A. Investigation Of Propane And Methane Bulk Properties Structure Using Two Different Force Fields. *Lect. Notes Comput. Sc.* **2008**, *5072*, 1052-1064.

(41) Costantini, A.; Gutierrez, E.; López-Cacheiro, J.; Rodríguez, A.; Gervasi, O.; Laganà, A. Porting Of GROMACS Package Into The Grid Environment: Testing Of A New Distribution Strategy. *Lect. Notes Comput. Sc.* **2010**, *6019*, 41-52.

(42) Gervasi, O.; Riganelli, A.; Pacifici, L.; Laganà, A. VMSLab-G: A Virtual Laboratory Prototype For Molecular Science On The Grid. *Future Gener. Comp. Sys.* **2004**, *20*, 717-726.

(43) Hase, W. L.; Duchovic, R. J.; Hu, X.; Komornicki, A.; Lim, K. F.; Lu, D.; Peslherbe, G. H.; Swamy, K. N.; Van de Linde, S. R.; Varandas, A. J. C.; Wang, H.; Wolf, R. J. VENUS96: A General Chemical Dynamics Computer Program. *QCPE Bull.* **1996**, *16*, 43.

(44) Laganà, A.; Garcia, E.; Paladini, A.; Casavecchia, P.; Balucani, N. The Last Mile Of Molecular Reaction Dynamics Virtual Experiments: The Case Of OH(N=1-10) + CO(j=0-3) Reaction. *Faraday Discuss.* **2012**, *157*, 415-436.

(45) European Grid Infrastructure. `http://www.egi.eu` (accessed Ago 10, 2015).

(46) Erl, T. *Service Oriented Architecture: Concepts, Technology and Design*; Prentice Hall: Upper Saddle River, NJ, USA, 2005.

(47) Esposito, F.; Armenise, I.; Capitta, G.; Capitelli, M. O+O_2 State-to-State Vibrational Relaxation And Dissociation Rates Based On Quasiclassical Calculations. *Chem. Phys.* **2008**, *351*, 91-98.

(48) Kučera, M.; Stano, M.; Wnorowska, J.; Barszczewska, W.; Loffhagen, D.; Matejčík, Š. Electron Attachment To Oxygen In Nitrogen Buffer Gas At Atmospheric Pressure. *Eur. Phys. J. D* **2013**, *67*, 234 (8 pages).

Graphical TOC Entry